TITLE: Harnessing the regenerative potential of *interleukin11* to enhance heart repair

AUTHORS: Kwangdeok Shin[1], Anjelica Rodriguez-Parks[1], Chanul Kim[1], Isabella M. Silaban[1], Yu Xia[3], Jisheng Sun[5], Chenyang Dong[4], Sunduz Keles[4], Jinhu Wang[5], Jingli Cao[3], Junsu Kang[1,2]

AFFILIATIONS

[1]Department of Cell and Regenerative Biology, School of Medicine and Public Health, University of Wisconsin - Madison, Madison, WI, 53705, USA.

[2]UW Carbone Cancer Center, School of Medicine and Public Health, University of Wisconsin - Madison, Madison, WI, 53705, USA

[3]Cardiovascular Research Institute, Department of Cell and Developmental Biology, Weill Cornell Medical College, New York, NY, 10065, USA.

[4]Departments of Statistics and of Biostatistics and Medical Informatics, University of Wisconsin - Madison, Madison, WI 53706, USA.

[5]Cardiology Division, School of Medicine, Emory University, Atlanta, GA 30322, USA.

ABSTRACT

Balancing between regenerative processes and fibrosis is crucial for heart repair, yet strategies regulating this balance remain a barrier to developing therapies. While Interleukin11 (IL11) is known as a fibrotic factor, its contribution to heart regeneration is poorly understood. We uncovered that *il11a, an Il11* homolog in zebrafish, can trigger robust regenerative programs in zebrafish hearts, including cardiomyocytes proliferation and coronary expansion, even in the absence of injury. However, prolonged *il11a* induction in uninjured hearts causes persistent fibroblast emergence, resulting in fibrosis. While deciphering the regenerative and fibrotic effects of *il11a*, we found that *il11*-dependent fibrosis, but not regeneration, is mediated through ERK activity, suggesting to potentially uncouple *il11a* dual effects on regeneration and fibrosis. To harness the *il11a*'s regenerative ability, we devised a combinatorial treatment through *il11a* induction with ERK inhibition. This approach enhances cardiomyocyte proliferation with mitigated fibrosis, achieving a balance between regenerative processes and fibrosis. Thus, we unveil the mechanistic insights into regenerative *il11* roles, offering therapeutic avenues to foster cardiac repair without exacerbating fibrosis.

INTRODUCTION

Unlike adult mammals, adult zebrafish possess the remarkable capacity to regenerate lost cardiac tissues upon injury [1, 2]. This regenerative ability of cardiac muscle cells can be achieved by dedifferentiation and proliferation of pre-existing cardiomyocytes (CMs) [3, 4, 5]. The regenerative events in CMs are orchestrated by molecular signals provided by activated non-muscular cells, including epicardium, endocardium, and immune cells, which create a regenerative niche [3, 6, 7, 8, 9, 10, 11, 12]. Furthermore, similar to injured mammalian hearts, zebrafish exhibit an acute response to cardiac injury by depositing extracellular matrix (ECM) proteins at the injury site [13]. Although fibrosis is generally considered detrimental to regeneration, cardiac fibrosis is a double-edged event for heart regeneration as it plays a critical function to prevent rupture during the early phase of heart regeneration [13, 14, 15]. Indeed, preventing fibrosis during the early phase of the injured zebrafish hearts leads to defective heart repair [13]. In opposition to mammals, the cardiac fibrotic tissue in zebrafish hearts transiently form and are eventually replaced by newly formed CMs [16, 17]. Therefore, dissecting the key signaling pathways governing regeneration and fibrosis is vital to understand the intricate processes of heart regeneration.

RESULTS

Dynamics of endogenous *il11a* expression during zebrafish heart regeneration

Interleukin11 (IL11), a pleiotropic cytokine of the IL-6 family, plays regenerative roles in multiple injury contexts [18, 19, 20]. To investigate roles of *il11a*, one of two *il11* zebrafish homologs, in zebrafish hearts, we analyzed its expression with a newly created

knock-in reporter line, *il11a*^{EGFP} **(Fig. 1a, b and Supplementary Fig. 1a).** *il11a*^{EGFP} expression is undetectable in uninjured hearts of embryonic and adult hearts **(Fig. 1a, b and Supplementary Fig. 1b, c)**, suggesting its minimal contribution to heart development and homeostasis. Upon cardiac injury, *il11a* is robustly induced from non-CMs, primarily epicardium and endocardium **(Fig. 1a-d and Supplementary Fig. 1b, c)**. *il11a*^{EGFP} expression was detectable as early as 1 dpa, highly and widely induced at 3 dpa throughout the ventricle, became localized to the wound site at 7 dpa, and largely undetectable by 14 dpa **(Fig. 1a, b)**. Additionally, our further analysis to dissect *il11a* expressing cells revealed that epicardial *il11a*^{EGFP} expression decreased, whereas endocardial expression at the wound area remained constant from 3 to 7 dpa. **(Supplementary Fig. 1d, e)**. The robust and prompt *il11a*^{EGFP} expression throughout the ventricle during the early phase of regeneration suggests its potential influence on the activation of non-CMs, whereas wound-restricted *il11a*^{EGFP} expression during the mid-phase of regeneration indicates a potential interaction between *il11a* signaling and CMs for their renewal. The diminished expression of *il11a* by 14 dpa indicates the minimal contribution of *il11a* during the late phase of regeneration **(Supplementary Fig. 1f, g)**.

il11a induction can promote cardiomyocyte proliferation in uninjured hearts

Previous studies of *il11* signaling in zebrafish hearts mainly focused on loss-of-function experiments with mutants of *il11* signaling components, such as *il11ra*, revealing impaired regeneration in the mutant hearts [21]. In rodents, *Il11* roles on cardiac fibrosis have been reported, but its regenerative roles remain unclear [22, 23, 24]. To our knowledge, there has been no comprehensive analysis of *il11* functionality on cell cycle reentry of

CMs. To address this, we developed a new transgenic line*, Tg(actb2:loxp-BFP-STOP-loxp-il11a*), or *actb2:BS-il11a*, which allowed conditional overexpression (OE) of *il11a* in combination with *CreER* line. Crossing with *cmlc2:CreER*, we induced *il11a*OE from cardiac muscle cells upon tamoxifen treatment in the absence of injury **(Fig. 2a)**. Notably, *il11a*OE led to the marked induction of cell cycle reentry in CM of the uninjured hearts, whereas control hearts showed little to no cell cycle activity in CMs **(Fig. 2b, d).** Moreover, we noted a significant induction of phospho-H3 (pH3) positive CMs in the uninjured *il11a*OE hearts, compared to control **(Supplementary Fig. 2a, b)**, suggesting that *il11a*OE is sufficient to trigger CM proliferation. *il11a*-triggered CM proliferation could be caused by cell death or damages. To test this possibility, we performed Terminal deoxynucleotidyl transferase (TdT) dUTP Nick-End Labeling (TUNEL) assay and found that TUNEL$^+$ cells are undetectable in *il11a*OE hearts, while our control experiment with cryoinjured hearts displayed robust TUNEL$^+$ cells at 7 days post-cryoinjury (dpi) **(Supplementary Fig. 3)**. Our results indicate that *il11a*OE unlikely induces apoptosis but directly triggers CM proliferation.

We next analyzed bulk RNA-seq profiles with control and *il11a*OE ventricles at 7 days post-treatment (dpt), identifying 1,327 genes (n = 862 and 465 for up- and down-regulated genes, respectively) with significantly changed expression levels (adjusted P [P-adj] < 0.05; fold change > 4) **(Supplementary Fig. 2c and Supplementary Data 1).** *il11a*OE upregulated regeneration-associated genes, including a regeneration-specific factor (*lepb),* pro-regenerative ECM proteins (*fn1b, hmmr,* and *col12a1b),* and cell cycle genes (*plk1, cdk1, ccnb1, ccnb2, and mki67*), indicating activated regeneration response by *il11a* induction [3, 25, 26, 27, 28]. Gene ontology (GO) analyses with up-regulated genes in

*il11a*OE hearts revealed enrichment in cell cycle, nuclear division, and DNA replication, highlighting active proliferation **(Supplementary Fig. 2d)**. Additionally, gene set enrichment analysis (GSEA) identified significant enrichment of cell cycle signature in *il11a*OE **(Supplementary Fig. 2e)**. *il11a* induction also highly upregulated key components of janus kinase/signal transducers and activators of transcription (JAK/STAT) signaling pathway, including *jak1, stat3*, and *socs3b,* which constitute a canonical downstream pathway of IL11 [29, 30, 31] **(Supplementary Fig. 4a)**. Our *in situ* hybridization (ISH) analysis further confirmed that JAK/STAT-related factors are highly upregulated in CMs upon *il11a* induction **(Supplementary Fig. 4b)**. Moreover, *il11a*OE robustly increased phospho-STAT3 (p-STAT3) labelled CMs and 5.87% of pSTAT-3$^+$ Mef2$^+$ CMs are labelled by EdU, suggesting the active STAT3 pathway in CMs **(Supplementary Fig. 4c, d)**.

To re-enter cell cycle, CMs undergo dedifferentiation, characterized by sarcomere disassembly and downregulation of genes associated with mature CMs [4, 32, 33, 34]. Indeed, the down-regulated genes in response to *il11a* induction are primarily associated with cardiac muscle contraction and metabolic processes **(Supplementary Fig. 2d, f)**, suggesting a transcriptional shift from a mature to an immature state in CMs upon *il11a* induction. We next assessed the impact on sarcomere structure through α-actinin staining in control and *il11a*OE at 30 dpt. While control hearts displayed no sign of dedifferentiated CMs**,** *il11a*OE hearts exhibited a markedly increased sarcomere disassembly with blurred Z-discs **(Fig. 2c, e)**. To evaluate the long-term mitogenic effect of *il11a*OE, we analyzed the uninjured hearts at 3 and 7 months post-tamoxifen treatment (mpt). While no differences in body size and weight were observed between control and *il11a*OE

(Supplementary Fig. 5), *il11a*OE hearts displayed a noticeable enlargement with a 20% increase in size at 3 mpt **(Fig. 2f, g)** and the significantly augmented size of the ventricles at 7 mpt **(Fig. 2f)**, indicative of cardiomegaly.

Enlarged hearts can be caused by cardiac hypertrophy, a prominent mechanism responsible for the augmented mammalian hearts following injury [35], or hyperplasia, a desirable regenerative feature. To determine hypertrophic or hyperplastic effect of *il11a* induction, we quantified the CM density in the ventricles. The number of Mef2$^+$ nuclei in the ventricle significantly increased in *il11a*OE, compared to control (123.45 ± 8.71 and 107.45 ± 12.23 CMs / 4 x 10^4 μm^2 for *il11a*OE and control, respectively) **(Fig. 2h, i)**. Additionally, the individual CMs isolated from *il11a*OE hearts exhibited smaller length (83.65 ± 23.5 μm) than control (101.2 ± 23.2 μm) **(Fig. 2j, l)**. While there is no notable difference in width between control and *il11a*OE CMs, *il11a*OE hearts likely contain some enlarged CMs, indicating a possible low level of hypertrophic effect **(Fig. 2j, k)**. Collectively, these results indicate that *il11a* activation can lead to notable myocardial hyperplasia, highlighting its regenerative effect in zebrafish hearts.

il11a overexpression hypervascularizes the uninjured zebrafish hearts

Stimulating revascularization of coronary vessels is a crucial regenerative process for the hearts [36, 37, 38]. To determine whether *il11a*OE can promote coronary vascularization in the absence of injury, we examined the coronary network using *fli1a:EGFP*$^+$, which labels endothelial vessels [39, 40]. Remarkably, whole-mount images demonstrated a more elaborate *fli1a*:EGFP$^+$ coronary network in the *il11a*OE hearts as significantly increased vessel density was observed in *il11a*OE ventricles (18.84 ± 4.98%

to 26.34% ± 3.27%) **(Fig. 3a, b)**. *fli1a*:EGFP$^+$ area in the cortical layer is also highly enhanced in *il11a*OE hearts (10.58 ± 1.19%), compared to control (6.78 ± 0.8%) **(Fig. 3c, d)**. Our transcriptome data revealed that *il11a*OE hearts exhibit a significant upregulation of genes associated with vascularization, including *angptl2a, emilin2a, hmmr, rspo3, sulf1,* and *thsd7aa* [37, 41, 42, 43, 44, 45] **(Supplementary Fig. 6a)**. Our scRNA-seq analysis with published dataset of regenerating hearts [44] identified their injury-dependent induction predominantly within the epicardial cell clusters **(Fig. 3e and Supplementary Fig. 6b-d)**. Our ISH analysis also validated that the angiogenic factors are highly upregulated in the epicardial and cortical layer in *il11a*OE, but not in control **(Fig. 3f)**. Given the pivotal role of the epicardium in guiding coronary growth [8, 37, 41, 46], alongside with angiogenic factor increment by *il11a*, our data suggest that *il11a* induction activates epicardium to facilitate coronary growth.

While epicardium is normally quiescent in uninjured hearts, cardiac injury activates epicardium to undergo epithelial-to-mesenchymal transition (EMT) [47, 48], giving rise to epicardial progenitor cells (EPCs), which are marked by *col12a1b* expression [49, 50]. These EPCs subsequently differentiate into diverse epicardium-derived cells (EPDCs) in regenerating hearts [49]. We thus examined whether *il11a* induction can activate the dormant epicardium to initiate the generation of *col12a1b*$^+$ EPCs even in the uninjured hearts. In control hearts, *tcf21*$^+$ epithelial cells are typically restricted to one or two layers outlining the ventricles. In contrast, within *il11a*OE hearts, *tcf21*$^+$ layers expanded into the mesenchymal layers, a deeper region of the cortical wall, indicating that *il11a* induction triggers the epicardium to undergo EMT **(Fig. 3g)**. Evidently, a subset of *tcf21*$^+$ epicardial cells within *il11a*OE hearts display *col12a1b:EGFP* expression at 10 dpt, indicating that

il11a induction activates *tcf21*$^{+}$ epicardial cells to become EPCs **(Fig. 3g)**. By 30 dpt, *il11a*OE hearts displayed extensive expansion of *col12a1b*$^{+}$ EPC populations within the deeper mesenchymal layer **(Fig. 3g)**. In contrast, *col12a1b*$^{+}$ EPCs were conspicuously absent in control hearts at 10 and 30 dpt. We also tested whether *il11a*OE can stimulate the activation of *hapln1b*$^{+}$ EPDCs as *hapln1*$^{+}$ EPDCs are known to impact coronary growth [8]. Our data revealed that *il11a*OE hearts display the expansion of *hapln1b*$^{+}$ cell populations in the mesenchymal layer at 30 dpt **(Fig. 3h, i)**. Therefore, our results indicate that *il11a* can stimulate the epicardium to generate EPCs which subsequently differentiate into EPDCs impacting coronary vascularization.

The cardiac fibrotic effects of prolonged *il11a* treatment

Given recent reports indicating IL11 as a fibrotic factor [22, 23, 24], we explored whether *il11a* could exert a fibrotic role in zebrafish hearts. At 30 dpt, there is no significant difference of collagen deposition between control and *il11a*OE hearts **(Fig. 4a)**. While fibrotic tissue was undetectable in control hearts, *il11a*OE hearts exhibited collagen accumulation in the cortical layer by 3 mpt and massive collagen deposition by 7 mpt **(Fig. 4a, b)**. The cardiac fibrosis mainly manifested in the cortical layer and surface, rather than within the ventricles, and its thickness expanded over time **(Fig. 4a, b)**. These findings suggest that long-term *il11a* induction leads to cardiac fibrosis, especially in the cortical layer.

To assess the induction of fibrosis-associated genes by prolonged *il11a*OE, we performed RNA-seq analysis with 7 mpt control and *il11a*OE hearts, comparing them with 7 dpt transcriptome datasets. The border zone of the injured hearts exhibits high

enrichment of embryonic CM genes, including *nppa, nppb, desma*, and *ankrd1a* [51, 52, 53]. These embryonic genes, in addition to cell cycle and regenerative ECM genes **(Supplementary Fig. 2c and 7a)**, are upregulated early at 7 dpt after *il11a* induction, suggesting the prompt regenerative effect of *il11a* in hearts **(Supplementary Fig. 7a)**. By contrast, our transcriptome analysis revealed a significant upregulation of pathological fibrotic and cardiac fibroblast marker genes, including *col1a1a/b, col5a1, postnb, sox9a/b, dcn,* fibroblast activation genes (*cthrc1a, thbs4b*), ECM-linking genes (various Lysyl oxidase (LOX) enzymes), ECM maturation genes (*mgp, sparc*) and in 7 mpt *il11a*OE hearts, but not 7 dpt **(Fig. 4c, Supplementary Fig. 7a, b, and Supplementary Data 1 and 2)** [13, 54, 55, 56, 57, 58, 59, 60, 61, 62 59, 60, 61, 62]. Extended *il11a* induction moderately, but not robustly, upregulates one of two *transforming growth factor β1* (*tgfb1*) homologs **(Supplementary Fig. 7a)**, aligning with the previous finding that *Il11* plays roles as a downstream effector of *Tgfb1* for cardiac fibrosis [22]. These results highlight the dual functions of *il11* as a regenerative factor with more immediate effects and a fibrotic factor, presumably, with indirect consequences.

In regenerating zebrafish hearts, cardiac fibrosis is largely mediated by epicardium-derived fibroblasts that appear in the cortical layer following injury [6, 13, 63, 64]. Given that the fibrosis driven by *il11a* is predominantly observed in this cortical layer, we hypothesize that prolonged *il11a* exposure can activate the epicardium constantly, leading to sustained cardiac fibroblast production and subsequent fibrosis. Supporting this notion, while Periostin$^+$ (Postn$^+$) cells are undetectable in the 10 dpt *il11a*OE hearts, *il11a* induction led to the emergence of Postn$^+$ fibroblasts in the cortical layer at 30 dpt without an injury **(Fig. 4d, e)**. These Postn$^+$ fibroblasts are gradually expanded at 3 mpt

and dispersed across the cortical layer, where collagens are extensively deposited. Next, we examined whether epicardial cells can give rise to the Postn $^{+}$ fibroblasts. Notably, 66% Postn^{+} cells are colocalized with *tcf21*:mCherry^{+} epicardial cells in *il11a*OE at 30 dpt while there is no Postn expression in epicardial cells of control hearts **(Fig. 4f, g)**. Thus, our results indicate that *il11a*-induced fibrosis is mediated by epicardial-derived Postn^{+} cardiac fibroblasts**.**

ACTA2, smooth muscle alpha (α)-2 actin, is used as a biomarker for the injury-induced myofibroblasts in mammalian hearts [65, 66], raising a question of ACTA2 expression in response to *il11a*OE. In addition to myofibroblasts, ACTA2 also labels vascular smooth muscle cells (VSMCs) and dedifferentiating CMs [51, 67]. While circular ACTA2^{+} cell layers were observed in the cortical layers of both control and *il11a*OE hearts, *il11a* induced the additional ACTA2^{+} cells in the cortical layer without an injury at 30 dpt (**Supplementary Fig. 8a-e)**. To discriminate ACTA2-expressing cells, we examined their location and colocalization with blood vessels and CM markers. In control hearts, most ACTA2^{+} cells were found encircling *fil1a:EGFP*$^{+}$ coronary vessels within the outer cortical layer of ventricles, an indicative of VSMC **(Supplementary Fig. 8c**). Although circular ACTA2^{+} VSMC layers were also evident in *il11a*OE hearts, we found that *il11a*OE hearts additionally display a thick and linear ACTA2^{+} layer in the deeper cortical layer (**Supplementary Fig. 8c**). These ACTA2^{+} layers are not closely associated with *fli1a:EGFP*$^{+}$ cells, indicating non-VSMC cell types **(Supplementary Fig. 8d**). While the majority of these ACTA2^{+} cells lack α-actinin CM signature **(Supplementary Fig. 8e)**, they co-express a myosin heavy chain (MHC) CM gene **(Supplementary Fig. 8f-h)**. Based on the anatomical location of the primordial CM layer that gives rise to trabecular

CMs during development [68], our results indicate that *il11a*-induced ACTA2$^+$ layers in the deeper cortical layer are likely dedifferentiating CMs.

As ERK, a downstream effector of the MAPK pathway, controls various cellular processes, including proliferation, survival, and fibrosis [69, 70], we questioned whether ERK mediates *il11a*-inducible fibrosis in the epicardium. While control hearts contain a minimal number of phospho-ERK (pERK)$^+$ *tcf21*$^+$ epicardial cells, their numbers are significantly increased upon *il11a* induction **(Fig. 4h, i and Supplementary Fig. 7c, d)**. Also, the pERK signal remained undetectable in CMs in both control and *il11a*OE **(Supplementary Fig. 7e)**, indicating the limited impact of MAPK/ERK signaling on CM proliferation. These findings suggest that the persistent *il11a* induction can provoke fibrosis by promoting the presence of cardiac fibroblasts from MAPK/ERK-activated EPCs.

il11a induction with ERK inhibition can enhance CM proliferation without exacerbating fibrosis

Our studies on *il11a*OE in uninjured hearts demonstrated dual roles of *il11a,* acting as a double-edged sword in heart repair: *il11* signaling can promote the regenerative program while also contributing to cardiac fibrosis **(Fig. 4j)**. We next explored whether this dual functionality of *il11a* is also operational in injured hearts. At 14 days post-injured hearts, ectopic *il11a* activation significantly increased CM cycling (8.61 ± 1.26 % and 5.20 ± 0.80 % in OE and control, respectively) **(Fig. 5a, b and Supplementary Fig. 9a)**, confirming its regenerative effect on injured hearts. To assess the fibrotic effects of *il11a* on injured hearts, we performed ventricular apex resection with control and *il11a*OE fish and collected hearts at 30 dpa, at which myocardial wall regeneration is typically

completed [1]. Control hearts had limited scarring at the wound, a sign of successful scar resolution. In contrast, *il11a*OE hearts exhibited apparent collagen-rich scar tissues at the injury site (8.19 ± 3.33 % and 0.62 ± 0.67 % in OE and control, respectively) **(Fig. 5c, d and Supplementary Fig. 9b, c)**. This time point is relatively earlier than when *il11a*-stimulated fibrosis is observed in the uninjured hearts, as uninjured *il11a*OE hearts did not display noticeable collagen-rich fibrotic tissues at 30 dpt **(Fig. 4a)**. Furthermore, ectopic *il11a* induction led to the persistence of *col12a1b*$^{+}$ EPCs and fibrotic tissues at the injury site in cryoinjured hearts **(Supplementary Fig. 10a-d)**. Similar to *il11a*OE uninjured hearts, we observed prominent Postn^{+} layers at the wound area of *il11a*OE hearts, suggesting the existence of cardiac fibroblasts induced by *il11a*OE. **(Supplementary Fig. 10e, f)**. Overall, these results indicate regenerative and fibrotic functions of *il11a* in injured hearts.

To harness the regenerative potential of *il11a* for injured hearts, mitigating its fibrotic function is crucial. Thus, we devised a concurrent treatment strategy involving *il11a* induction with preventing cardiac fibrosis through ERK/MAPK inhibition **(Fig. 5e)**. This approach aims to facilitate heart repair by promoting CM proliferation via *il11a* induction while minimizing cardiac fibrosis by inhibiting fibrosis-specific signaling at a later time point. To achieve this, we administered U0126, an ERK inhibitor [71], for a month, starting at 2 weeks after cryoinjury with control and *il11a*OE fish and collected hearts at 45 days post-injury (dpi) **(Fig. 5f)**. Collagen deposition was not evident in the hearts of control fish treated with vehicle or U0126 **(Fig. 5g, h)**, suggesting that U0126 treatment during the late regenerative phase minimally affects heart repair. By contrast, *il11a*OE hearts treated with vehicle displayed significant collagen deposition at the injury site,

confirming the fibrotic function of *il11a* in injured hearts **(Fig. 5g, h)**. Interestingly, U0126 treatment in *il11a*OE significantly reduced the presence of fibrotic tissues at the injury site **(Fig. 5g, h)**, implicating that inhibiting ERK activity reduces *il11a*-induced cardiac fibrosis. Moreover, we observed that CMs in *il11a*OE hearts treated with U0126 and vehicle exhibited a similar cell cycling rate **(Fig. 5i, j)**. As another readout of regeneration, we quantified the total number of Mef2$^+$ CMs throughout a ventricle in 45 dpi hearts and found that U0126-treated *il11a*OE hearts have significantly more Mef2$^+$ CMs than control hearts (**Supplementary Fig. 11a, b**). These results highlight the specific effect of ERK/MAPK inhibition on cardiac fibrosis with limited influence on regeneration. Taken together, our findings provide a proof-of-principle that combinatorial treatment of *il11a* induction with inhibiting fibrosis holds significant potential for enhancing heart regeneration following cardiac injury.

DISCUSSION

Our expression analysis and functional assays shed light on that *il11* is a potent regenerative factor for heart repair. During normal heart regeneration, *il11a* is produced from non-CMs at the early phase to trigger regenerative programs by initiating cell cycle reentry for CMs, activating epicardium for generating EPCs, and stimulating vascularization. Its expression is decommissioned at the late regenerative phase to block aberrant outcomes, such as preventing fibrosis resolution. We demonstrate that *il11a* induction in the uninjured heart can stimulate regeneration programs, indicating that *il11* is a potent regenerative factor to enhance heart repair. Notably, we showed that *il11a* induction can enlarge hearts via CM hyperplasia rather than hypertrophy. However,

prolonged epicardium activation by *il11a* leads to the persistent presence of EPCs, resulting in the constant production of cardiac fibroblasts and subsequent fibrosis. Additionally, our analysis of scRNA-seq profiles obtained from an extensive number of cardiac cells[44] revealed widespread expression of *il11ra,* a zebrafish homolog of *il11* receptor gene, across multiple cardiac cell types, including CMs and epicardium, supporting the pivotal function of IL11 signaling in CMs and epicardium (**Supplementary Fig. 11c)**. Overall, our study demonstrates that *il11* signaling should be tightly regulated for effective and successful heart regeneration.

Regenerative paracrine factors are promising therapeutic candidates, due to their potential efficacy as drugs and simple delivery methods. Cytosolic and nuclear proteins require specific methodologies to be delivered inside the cells, presenting an additional challenge [72, 73, 74]. However, our studies reveal that application of paracrine factors for heart regeneration should be carefully considered, especially in the aspect of cardiac fibrosis. One essential yet paradoxical regenerative event is to accumulate ECM proteins, such as collagen, by cardiac fibroblasts at the injury site. Although this fibrotic response is thought to be detrimental due to its non-contractile feature potentially causing heart failure [75], it is indispensable and beneficial for heart regeneration at the early phase [13, 76, 77]. As demonstrated in our study, a single paracrine factor and signaling can target multiple cardiac cells, including CMs, endocardium/endothelium, and epicardium. Notably, the activated epicardial cells undergo reprogramming to generate progenitor cells, which later differentiate into the cardiac fibroblasts contributing to fibrosis. Consequently, a paracrine factor can serve as a double-edged sword to induce beneficial regenerative effects as well as detrimental cardiac fibrosis. In nature, these two effects

are precisely balanced through tight spatiotemporal control during heart regeneration. However, current methodologies to enhance heart regeneration often face limitations, such as targeting multiple cell types by viral vectors or delivery vehicles [78], and obscure duration for functional recovery [79]. Here, we prove that delivering *il11a* paracrine factor, along with inhibiting cardiac fibrosis via ERK inhibitor treatment, in injured hearts can maintain CM proliferation without exacerbating fibrosis. Therefore, paracrine factor treatment combined with attenuating cardiac fibrosis can represent a more effective regenerative medicine strategy.

Previous works on *il11* across animal species and tissues have revealed seemingly conflicting results, as *il11* is known to have both regenerative and fibrotic properties [18, 19, 20, 21, 22, 23, 30, 80, 81, 82, 83, 84, 85]. Regarding the hearts, cardioprotective and fibrotic roles of *Il11* have been reported [21, 22, 23, 30, 84, 85]. Both *il11ra* mutant (loss-of-function for IL11 signaling) [21] and *il11*OE (gain-of-function in this work and Ref. 85)[85] models exhibited cardiac fibrosis phenotypes. Loss-of-function study demonstrated that *il11ra* mutants exhibit an elevated number of myofibroblasts derived from endocardium and epicardium, leading to defective resolution of cardiac fibrosis. Tissue-specific rescue experiment of *il11ra* mitigates endocardium-derived myofibroblast differentiation, but not epicardium, suggesting the key roles of *il11* signaling in the endocardium for endothelial-to-mesenchymal transition (EndoMT). Our gain-of-function study revealed that *il11a*-mediated fibrotic effect is indirect through prolonged activation of epicardium. *il11*-induced epicardial activation is crucial to establish a regenerative niche at the initial phase of regeneration. However, persistent epicardium activation by *il11* results in continuous generation of cardiac fibroblasts, ultimately leading to cardiac fibrosis. These findings can

explain controversies of *il11* signaling by highlighting pleiotropic function of *il11* depending on the location and duration of its expression.

Our study offers important new insights into IL11 biology for cardiac regeneration and fibrosis. A deeper understanding of IL11-associated cellular and molecular processes will be critical for developing a therapeutic strategy for precise regenerative effects with limited fibrosis.

METHODS

Zebrafish

Wild-type or transgenic male and female zebrafish of the outbred Ekkwill (EK) strain ranging up to 18 months of age were used for all zebrafish experiments. The following transgenic lines were used in this study: *Tg(cmlc2:creER)*^{pd10}, *Tg(cmlc2:mCherry-N-2A-Fluc)*^{pd71}, *Tg(col12a1b:EGFP)*^{wcm108}, *Tg(fli1:EGFP)*^{y1}, *Tg(−6.5kdrl:mCherry)*^{ci5}, *Tg(tcf21:mCherry-NTR)*^{pd108}, *hapln1b*:EGFP [4, 49, 50, 86, 87, 88, 89]. To generate *actb2:loxP-BFP-loxP-il11a* (*uwk28*), the transgenic construct was generated by modifying *actb2:loxP-BFP-loxP-nrg1* [90]. The *nrg1* sequence were replaced with *il11a* cDNA amplified by PCR using wild-type zebrafish cDNA libraries. Primers are listed in **Supplementary Table 1**. The entire cassette was flanked with I-*Sce*I sites for meganusclease-enhanced transgenesis. The identified founder line was crossed with *cmlc2:creER* to induce *il11a* induction upon tamoxifen treatment. Water temperature was maintained at 26°C for animals unless otherwise indicated. Work with zebrafish was performed in accordance with University of Wisconsin-Madison guidelines. Partial ventricular resention surgery was performed as described previously [1], in which ~20% of the cardiac ventricle was removed at the apex. Ventricular cryoinjuries were performed as described [91]. Briefly, the ventricular wall was applied by a cryoprobe precooled in liquid nitrogen.

Generation of *il11a*^{EGFP}

To generate *il11a* knock-in reporter (*uwk25*), we generated a donor construct having 5' and 3' homology arms (HAs) and *EGFP-SV40pA* cassette. 5' and 3' HAs were amplified

using genomic DNA extracted from fish that were used for injection. These HA fragments were subcloned into the pCS2-EGFP-pA-IsceI vector. For linearization, sgRNA located in 3' HA ("GG ATC AAGTG TTACT CGCTC AGG") was used. sgRNAs synthesis and microinjection were described in [92]. Briefly, sgRNA were synthesized by a cloning-free method using the MEGAshortscript T7 Transcription Kit (Invitrogen, AM1354) and purified by the RNA purification Kit (Zymogen, R1016) according to the manufacturer's instructions. A sgRNA (25~30 ng/ul) and a donor plasmid (20-25 ng/ul) were mixed and co-injected with Cas9 protein (0.5ug/ul; PNABio, CP01) into the one-cell stage embryos. After injection, none of larvae exhibit EGFP expression without injury. To sort F_0 animals carrying *EGFP-pA* at the *il11a* locus, fin folds were amputated at 3 or 4 dpf, and embryos displaying EGFP fluorescence near the injury site at 1 dpa were selected. EGFP positive larvae were raised to adulthood, and founders were screened with F_1 progenies driving fin fold injury-inducible EGFP expression. Integration at the *il11a* locus was identified by PCR with primers described in **Supplementary Table 1**, followed by Sanger sequencing. For expression pattern to determine spatiotemporal expression of $il11a^{EGFP}$, at least three biological replicates, unless indicated, were examined per each time point and per observation to allow for potential variability within a single experiment.

Immunostaining, histology and imaging

Hearts were fixed with 4% paraformaldehyde (PFA) for 1 hour at room temperature. Cryosectioning and immunohistochemistry were performed as described previously with modifications [25]. Hearts were cryosectioned at 10μm. Heart sections were equally distributed onto four to six serial slides so that each slide contained sections representing

all area of the ventricle. 5 or 10% goat serum, 1% BSA, 1% DMSO, and 0.2% Triton X-100 solution was used for blocking and antibody staining. The primary and secondary antibodies used in this study were: anti-myosin heavy chain (mouse, F59; Developmental Studies Hybridoma Bank; 1:50 or mouse, MF20; Developmental Studies Hybridoma Bank; 1:50), anti-EGFP (rabbit, A11122; Life Technologies; 1:200), anti-EGFP (chicken, GFP-1020; Aves Labs; 1:2000), anti-Ds-Red (rabbit, 632496; Clontech; 1:500), anti-mCherry (chicken, MC87977980; Aves Labs; 1:500), anti-Raldh2 (rabbit, GTX124302; Genetex; 1:200), anti-PCNA (mouse, P8825; Sigma; 1:200), anti-α-actinin (mouse, A7811; Sigma, 1:200), anti-ACTA2 (rabbit, GTX124505; GeneTex; 1:200), anti-pERK (rabbit, 9101; Cell Signaling Technology; 1:250). Anti-Mef2 (rabbit; 1:200) [49], Anti-phospho-Histone H3 (rabbit, 9701; Cell Signaling Technology, 1:100), Anti-phospho STAT3 (rabbit, 9131S; Cell Signaling Technology, 1:100), anti-Periostin (rabbit, 19899-1-AP, Proteintech, 1:200), Alexa Fluor 488 (mouse, rabbit, and chicken; A11029, A11034, and A11039; Life Technologies; 1:500), Alexa Fluor 594 (mouse and rabbit; A11032 and A11037; Life Technologies; 1:500). TUNEL staining was performed using in situ cell death detection kit (11684795910, Roche) in immunostaining. *In situ* hybridization (ISH) on cryosections of 4% paraformaldehyde-fixed hearts was performed as previously described [25]. To generate digoxigenin-labeled probes, we used cDNA for 3' part of each gene. Primer sequences are listed in **Supplementary Table 1**. Images of cardiac tissue sections were acquired using an Eclipse Ti-U inverted compound microscope (Nikon) or BZ-X810 fluorescence microscope (Keyence). Images were processed using either NIS-Elements (Nikon), ZEN (Zeiss), BZ-X800 analyzer (Keyence) or FIJI/ImageJ software.

AFOG staining and quantification of collagen deposition

AFOG staining was performed on 10 μm sections as described[1]. Samples were first incubated at 60°C for 2 hr with Bouin preheated at 60°C for 30 min; slides were then rinsed in running water for 30 min, and incubated with phosphomolybdic acid solution, followed by the sample incubation in AFGO staining solution for 10 min. For quantification of collagen deposition, collagen^{+} area was manually measured using ImageJ and normalized by the ventricular size and normalized by the entire ventricle size. Two to four largest sections were analyzed for each heart.

Drug treatment

For tamoxifen treatments, 6-month to 1-year-old adult zebrafish were bathed in 5 μM tamoxifen (Sigma-Aldrich, T5648) for 24 hr. zebrafish were rinsed with fresh aquarium water and returned to the recirculating water system for feeding. For 4-hydroxytamoxifen (4-HT) treatments, 6-month to 1-year-old adult zebrafish were intraperitoneally injected with 10 μl of 3mM 4-HT (Sigma-Aldrich, H7904) for 4 consecutive days and returned to the water system as described previously [93]. For EdU treatments, 10 mM EdU was intraperitoneally injected once every 24 hours for three consecutive days 24 hours prior to heart collection. For U0126 treatments, Fish were intraperitoneally injected with 10 μl of the 10 μM U0126 or 0.1 % DMSO in phosphate-buffered saline (PBS) using a 10 μl Hamilton syringe (1701SN) once daily for 30 days. CM ablation and imaging were performed as previously described in [94]. Briefly, 5 dpf *cmlc2:mCherry-NTR* zebrafish were incubated in 10 mM Metronidazole for 18 hours. The Mtz-containing medium was replaced with fresh embryo medium several times and larvae were returned to 28°C.

Whole mount imaging

Whole mount imaging was performed as described in [95]. Hearts were isolated from tricaine-anesthetized adult animals. Freshly isolated hearts were rinsed with 1X PBS and immediately mounted in 1% low-melting agarose/PBS (0.01% tricaine) in a glass bottom dish. The images were acquired using an Eclipse Ti-U inverted compound microscope (Nikon). Confocal sections covering the entire heart were imaged from ventral sides and processed to obtain maximal intensity projections. *Fli1a:EGFP*$^{+}$ area within a ventricle was assessed using ImageJ/Fiji image to measure vascular density.

Quantification of ventricular size

Hearts were collected from tricaine-anesthetized adult animals and fixed with 4% PFA for 1 hour at room temperature. Hearts were rinsed with 1X PBS with 0.1% Tween-20 and aligned on specimen stage. The images were acquired using an Zeiss Axio Zoom.V16 fluorescence stereo microscope. For quantification of ventricular size, the size was measured as described in [32]. the ventricular outline was manually traced, and the area encompassed by the outline was quantified using ZEN microscopy software (Blue edition).

Quantification of cardiomyocyte size

The size of cardiomyocytes was quantified as previously described in [32]. Zebrafish ventricles were fixed in 3% PFA for 5 min and incubated in PBS supplemented with 1 mg/mL collagenase type 4 (Worthington Biochemical) at 4°C overnight. Dissociated

cardiac muscle cells are deposited into a slide using a cytocentrifuge (Thermo Scientific, Cytospin 4), followed by immunofluorescence using an anti-α-actinin antibody. Images of α-actinin^{+} cells were acquired by BZ-X810 fluorescence microscope (Keyence) and used to measure the size of individual cardiomyocytes using FIJI/ImageJ software.

RNA isolation and bioinformatics

RNA was isolated from control and *il11a*OE hearts using Tri-Reagent (ThermoFisher). Complementary DNA (cDNA) was synthesized from 300 ng to 1 µg of total RNA using a NEB ProtoScript II first strand cDNA synthesis kit (NEB, E6560). For RNA-sequencing, total RNA was prepared from three biological replicate pools of 7 dpt or 7 mpt uninjured heart samples of control and *il11a*OE transgenic fish. Generation of mRNA libraries and sequencing were performed at the Biotechnology center at UW-Madison using an Illumina NovaSeq with 150 bp paired-end runs. Sequences were aligned to the zebrafish genome (GRCz11) using HISAT2 [96]. Differentially regulated transcripts were identified using Featurecount [97] and Deseq2 [98]. GO-term and GSEA analyses were done by the enrichGo and gseGO functions of clusterProfiler [99]. Accession numbers for transcriptome data sets are GEO233833.

scRNA-seq analysis of uninjured and regenerating hearts was done as described in [100]. Briefly, we obtained count files from GSE159032 and GSE158919 [44] and reanalyzed with Seurat package [101]. Low quality cells (nFeature_RNA ≥ 4100, mitoRatio ≥ 0.25) were filtered out. The 50 principal components (PCs) of the PCA with resolution 4 were used for clustering. Marker genes to identify cell-types are listed in [100].

Quantification of Mef2+ cells

Quantification of cardiomyocytes number in the ventricle was performed using the FIJI/ImageJ software. The entire ventricle region was determined and selected as a ROI with guidance provided by the green channel (α-actinin) images. To count the cardiomyocytes, red channel (Mef2) was converted to 8 bits in selected ROIs, followed by automatic count of the red circular objects with the Analyze Particles tool. The total numbers of cardiomyocytes in 5 serial cardiac sections were calculated.

Quantification

Quantification of EGFP$^+$ area was performed using the FIJI/ImageJ software. 2-5 sections were used to determine the values in one cardiac sample. ROIs were determined by manual selection of heart outlines, with guidance provided by the red channel (MHC) images. ROIs were selected by 400 μm (H) x 400 μm (W) from apex of a ventricle in the uninjured hearts or from amputation plane in the injured hearts. To quantify EGFP$^+$, selected ROIs were converted to 8 bit, adjusted with threshold, which is determined by autofluorescence level of EGFP$^+$ areas in ROIs were evaluated. For CM proliferation index, PCNA$^+$ Mef2$^+$ CMs were quantified from Mef2$^+$ CMs as described previously [11]. Images of the injury area were taken by 400 μm (W) x 200 μm (H) from the apical edge of the ventricular myocardium. The number of Mef2$^+$ PCNA$^+$ cells were manually counted using FIJI/ImageJ software. Three or four sections were analyzed for each heart. Quantification in uninjured hearts was conducted similarly, except that images of the mid-ventricular myocardium were taken for quantification. For quantification of sarcomere disorganization, 3 α-actinin$^+$ areas with 200 μm (W) x 200 μm (H) were randomly taken

from one section in the ventricular myocardium. The disorganized sarcomere area was manually measured by drawing a ROI without sarcomeric striation pattern. The sum of the ROIs was normalized by the entire α-actinin$^+$ area using FIJI/ImageJ software. For quantification of cardiomyocyte density, at least three area (200 μm (W) x 200 μm (H)) were randomly taken from the ventricular myocardium. The number of Mef2$^+$ cells were manually counted using FIJI/ImageJ software. For quantification of pERK$^+$ or Postn$^+$ area in *tcf21*:mCherry$^+$ area, ROIs were determined by red channel (mCherry) images and the green$^+$ (pERK or Postn$^+$) area in ROIs were evaluated.

Statistical values are represented as mean ± SD unless otherwise indicated. To determine the statistical significance, p values were calculated using unpaired t-tests unless otherwise indicated. p values are described in each figure legend.

DATA AVAILABILITY

Sequencing data have been deposited in GEO under accession code GEO233833. Reviewer token is qtqrwaqwhxkvpin.

ACKNOWLEDGMENTS

We thank UW-Madison School of Medicine and Public Health (SMPH) BRMS (Biomedical Research Models Services) staffs for zebrafish care; the University of Wisconsin Biotechnology Center DNA Sequencing Facility (Research Resource Identifier – RRID:SCR_017759) for providing RNA-seq services; Seungwon Ryu for assistance with sample preparation; and Jeffery F. Dilworth for comments on the manuscript.

COMPETING INTERESTS

The authors declare that they have no competing interests.

AUTHOR CONTRIBUTIONS

Biological experiments: KS, AR, YX, JS

Computational analysis and data curation: KS, CD, IMS, JK

Conceptualization: KS, JK

Writing original draft: KS, JK

Reviewing, Editing: KS, JK

Supervision: SK, JC, JK

Funding: JC, JK, JW

FUNDING:

National Institutes of Health grant R35 GM 137878 (JK)

National Institutes of Health grant R01 HL 151522 (JK)

National Institutes of Health, University of Wisconsin Carbone Cancer Center Support grant P30 CA 014520 (JK)

University of Wisconsin Institute for Clinical and Translational Research (UW ICTR) pilot grant (JK)

National Institutes of Health grant R01 HL 155607 (JC)

National Institutes of Health grant R01 HL 166518 (JC)

National Institutes of Health grant R01 HL 142762 (JW)

Stem Cell and Regenerative Medicine Center Research Training Award (KS)

REFERENCES

1. Poss KD, Wilson LG, Keating MT. Heart regeneration in zebrafish. *Science* **298**, 2188-2190 (2002).

2. Mehdipour M, Park S, Huang GN. Unlocking cardiomyocyte renewal potential for myocardial regeneration therapy. *Journal of molecular and cellular cardiology* **177**, 9-20 (2023).

3. Jopling C, Sleep E, Raya M, Marti M, Raya A, Izpisua Belmonte JC. Zebrafish heart regeneration occurs by cardiomyocyte dedifferentiation and proliferation. *Nature* **464**, 606-609 (2010).

4. Kikuchi K*, et al.* Primary contribution to zebrafish heart regeneration by gata4(+) cardiomyocytes. *Nature* **464**, 601-605 (2010).

5. Honkoop H*, et al.* Single-cell analysis uncovers that metabolic reprogramming by ErbB2 signaling is essential for cardiomyocyte proliferation in the regenerating heart. *eLife* **8**, (2019).

6. Wang J*, et al.* The regenerative capacity of zebrafish reverses cardiac failure caused by genetic cardiomyocyte depletion. *Development* **138**, 3421-3430 (2011).

7. Munch J, Grivas D, Gonzalez-Rajal A, Torregrosa-Carrion R, de la Pompa JL. Notch signalling restricts inflammation and serpine1 expression in the dynamic endocardium of the regenerating zebrafish heart. *Development* **144**, 1425-1440 (2017).

8. Sun J, Peterson EA, Chen X, Wang J. hapln1a(+) cells guide coronary growth during heart morphogenesis and regeneration. *Nat Commun* **14**, 3505 (2023).

9. Zhao L, Ben-Yair R, Burns CE, Burns CG. Endocardial Notch Signaling Promotes Cardiomyocyte Proliferation in the Regenerating Zebrafish Heart through Wnt Pathway Antagonism. *Cell Rep* **26**, 546-554 e545 (2019).

10. Wei KH*, et al.* Comparative single-cell profiling reveals distinct cardiac resident macrophages essential for zebrafish heart regeneration. *eLife* **12**, (2023).

11. Hui SP*, et al.* Zebrafish Regulatory T Cells Mediate Organ-Specific Regenerative Programs. *Developmental cell* **43**, 659-672 e655 (2017).

12. Tzahor E, Dimmeler S. A coalition to heal-the impact of the cardiac microenvironment. *Science* **377**, eabm4443 (2022).

13. Sanchez-Iranzo H*, et al.* Transient fibrosis resolves via fibroblast inactivation in the regenerating zebrafish heart. *Proceedings of the National Academy of Sciences of the United States of America* **115**, 4188-4193 (2018).

14. Kanisicak O*, et al.* Genetic lineage tracing defines myofibroblast origin and function in the injured heart. *Nat Commun* **7**, 12260 (2016).

15. Oka T*, et al.* Genetic manipulation of periostin expression reveals a role in cardiac hypertrophy and ventricular remodeling. *Circulation research* **101**, 313-321 (2007).

16. Gonzalez-Rosa JM, Martin V, Peralta M, Torres M, Mercader N. Extensive scar formation and regression during heart regeneration after cryoinjury in zebrafish. *Development* **138**, 1663-1674 (2011).

17. de Bakker DEM*, et al.* Prrx1b restricts fibrosis and promotes Nrg1-dependent cardiomyocyte proliferation during zebrafish heart regeneration. *Development* **148**, (2021).

18. Kirkiles-Smith NC*, et al.* IL-11 protects human microvascular endothelium from alloinjury in vivo by induction of survivin expression. *Journal of immunology* **172**, 1391-1396 (2004).

19. Yu J, Feng Z, Tan L, Pu L, Kong L. Interleukin-11 protects mouse liver from warm ischemia/reperfusion (WI/Rp) injury. *Clin Res Hepatol Gastroenterol* **40**, 562-570 (2016).

20. Tsujioka H, Kunieda T, Katou Y, Shirahige K, Fukazawa T, Kubo T. interleukin-11 induces and maintains progenitors of different cell lineages during Xenopus tadpole tail regeneration. *Nat Commun* **8**, 495 (2017).

21. Allanki S*, et al.* Interleukin-11 signaling promotes cellular reprogramming and limits fibrotic scarring during tissue regeneration. *Sci Adv* **7**, eabg6497 (2021).

22. Schafer S*, et al.* IL-11 is a crucial determinant of cardiovascular fibrosis. *Nature* **552**, 110-115 (2017).

23. Lim WW*, et al.* Antibody-mediated neutralization of IL11 signalling reduces ERK activation and cardiac fibrosis in a mouse model of severe pressure overload. *Clinical and experimental pharmacology & physiology* **48**, 605-613 (2021).

24. Corden B, Adami E, Sweeney M, Schafer S, Cook SA. IL-11 in cardiac and renal fibrosis: Late to the party but a central player. *British journal of pharmacology* **177**, 1695-1708 (2020).

25. Kang J*, et al.* Modulation of tissue repair by regeneration enhancer elements. *Nature* **532**, 201-206 (2016).

26. Wang J, Karra R, Dickson AL, Poss KD. Fibronectin is deposited by injury-activated epicardial cells and is necessary for zebrafish heart regeneration. *Developmental biology* **382**, 427-435 (2013).

27. Missinato MA, Tobita K, Romano N, Carroll JA, Tsang M. Extracellular component hyaluronic acid and its receptor Hmmr are required for epicardial EMT during heart regeneration. *Cardiovascular research* **107**, 487-498 (2015).

28. Mohamed TMA*, et al.* Regulation of Cell Cycle to Stimulate Adult Cardiomyocyte Proliferation and Cardiac Regeneration. *Cell* **173**, 104-116 e112 (2018).

29. Johnstone CN, Chand A, Putoczki TL, Ernst M. Emerging roles for IL-11 signaling in cancer development and progression: Focus on breast cancer. *Cytokine Growth Factor Rev* **26**, 489-498 (2015).

30. Obana M*, et al.* Therapeutic activation of signal transducer and activator of transcription 3 by interleukin-11 ameliorates cardiac fibrosis after myocardial infarction. *Circulation* **121**, 684-691 (2010).

31. Fang Y, Gupta V, Karra R, Holdway JE, Kikuchi K, Poss KD. Translational profiling of cardiomyocytes identifies an early Jak1/Stat3 injury response required for zebrafish heart regeneration. *Proceedings of the National Academy of Sciences of the United States of America* **110**, 13416-13421 (2013).

32. Ogawa M*, et al.* Kruppel-like factor 1 is a core cardiomyogenic trigger in zebrafish. *Science* **372**, 201-205 (2021).

33. Porrello ER*, et al.* Transient regenerative potential of the neonatal mouse heart. *Science* **331**, 1078-1080 (2011).

34. D'Uva G*, et al.* ERBB2 triggers mammalian heart regeneration by promoting cardiomyocyte dedifferentiation and proliferation. *Nature cell biology* **17**, 627-638 (2015).

35. Vasan RS, Larson MG, Benjamin EJ, Evans JC, Levy D. Left ventricular dilatation and the risk of congestive heart failure in people without myocardial infarction. *N Engl J Med* **336**, 1350-1355 (1997).

36. Marin-Juez R*, et al.* Fast revascularization of the injured area is essential to support zebrafish heart regeneration. *Proceedings of the National Academy of Sciences of the United States of America* **113**, 11237-11242 (2016).

37. Marin-Juez R*, et al.* Coronary Revascularization During Heart Regeneration Is Regulated by Epicardial and Endocardial Cues and Forms a Scaffold for Cardiomyocyte Repopulation. *Developmental cell* **51**, 503-515 e504 (2019).

38. Das S*, et al.* A Unique Collateral Artery Development Program Promotes Neonatal Heart Regeneration. *Cell* **176**, 1128-1142 e1118 (2019).

39. Harrison MR*, et al.* Chemokine-guided angiogenesis directs coronary vasculature formation in zebrafish. *Developmental cell* **33**, 442-454 (2015).

40. Harrison MR*, et al.* Late developing cardiac lymphatic vasculature supports adult zebrafish heart function and regeneration. *eLife* **8**, (2019).

41. El-Sammak H, Yang B, Guenther S, Chen W, Marin-Juez R, Stainier DYR. A Vegfc-Emilin2a-Cxcl8a Signaling Axis Required for Zebrafish Cardiac Regeneration. *Circulation research* **130**, 1014-1029 (2022).

42. Korf-Klingebiel M*, et al.* Heparan Sulfate-Editing Extracellular Sulfatases Enhance VEGF Bioavailability for Ischemic Heart Repair. *Circulation research* **125**, 787-801 (2019).

43. Scholz B*, et al.* Endothelial RSPO3 Controls Vascular Stability and Pruning through Non-canonical WNT/Ca(2+)/NFAT Signaling. *Developmental cell* **36**, 79-93 (2016).

44. Hu B*, et al.* Origin and function of activated fibroblast states during zebrafish heart regeneration. *Nature genetics* **54**, 1227-1237 (2022).

45. Liu LY*, et al.* Motor neuron-derived Thsd7a is essential for zebrafish vascular development via the Notch-dll4 signaling pathway. *J Biomed Sci* **23**, 59 (2016).

46. Zhou B*, et al.* Adult mouse epicardium modulates myocardial injury by secreting paracrine factors. *J Clin Invest* **121**, 1894-1904 (2011).

47. Quijada P, Trembley MA, Small EM. The Role of the Epicardium During Heart Development and Repair. *Circulation research* **126**, 377-394 (2020).

48. Cao J, Poss KD. The epicardium as a hub for heart regeneration. *Nat Rev Cardiol*, (2018).

49. Xia Y*, et al.* Activation of a transient progenitor state in the epicardium is required for zebrafish heart regeneration. *Nat Commun* **13**, 7704 (2022).

50. Sun J*, et al.* hapln1 Defines an Epicardial Cell Subpopulation Required for Cardiomyocyte Expansion During Heart Morphogenesis and Regeneration. *Circulation*, 101161CIRCULATIONAHA121055468 (2022).

51. Zhu Y, Do VD, Richards AM, Foo R. What we know about cardiomyocyte dedifferentiation. *Journal of molecular and cellular cardiology* **152**, 80-91 (2021).

52. Wu CC*, et al.* Spatially Resolved Genome-wide Transcriptional Profiling Identifies BMP Signaling as Essential Regulator of Zebrafish Cardiomyocyte Regeneration. *Developmental cell* **36**, 36-49 (2016).

53. van Duijvenboden K*, et al.* Conserved NPPB+ Border Zone Switches From MEF2- to AP-1-Driven Gene Program. *Circulation* **140**, 864-879 (2019).

54. Trogisch FA*, et al.* Endothelial cells drive organ fibrosis in mice by inducing expression of the transcription factor SOX9. *Science translational medicine* **16**, eabq4581 (2024).

55. Scharf GM*, et al.* Inactivation of Sox9 in fibroblasts reduces cardiac fibrosis and inflammation. *JCI Insight* **5**, (2019).

56. Lacraz GPA*, et al.* Tomo-Seq Identifies SOX9 as a Key Regulator of Cardiac Fibrosis During Ischemic Injury. *Circulation* **136**, 1396-1409 (2017).

57. Riley LA, Merryman WD. Cadherin-11 and cardiac fibrosis: A common target for a common pathology. *Cell Signal* **78**, 109876 (2021).

58. Davis J, Molkentin JD. Myofibroblasts: trust your heart and let fate decide. *Journal of molecular and cellular cardiology* **70**, 9-18 (2014).

59. Hua X*, et al.* Multi-level transcriptome sequencing identifies COL1A1 as a candidate marker in human heart failure progression. *BMC Med* **18**, 2 (2020).

60. Yokota T*, et al.* Type V Collagen in Scar Tissue Regulates the Size of Scar after Heart Injury. *Cell* **182**, 545-562 e523 (2020).

61. Williams L, Layton T, Yang N, Feldmann M, Nanchahal J. Collagen VI as a driver and disease biomarker in human fibrosis. *FEBS J* **289**, 3603-3629 (2022).

62. Xie T*, et al.* Single-Cell Deconvolution of Fibroblast Heterogeneity in Mouse Pulmonary Fibrosis. *Cell Rep* **22**, 3625-3640 (2018).

63. Gonzalez-Rosa JM, Peralta M, Mercader N. Pan-epicardial lineage tracing reveals that epicardium derived cells give rise to myofibroblasts and perivascular cells during zebrafish heart regeneration. *Developmental biology* **370**, 173-186 (2012).

64. Peralta M, Gonzalez-Rosa JM, Marques IJ, Mercader N. The Epicardium in the Embryonic and Adult Zebrafish. *J Dev Biol* **2**, 101-116 (2014).

65. Humeres C, Frangogiannis NG. Fibroblasts in the Infarcted, Remodeling, and Failing Heart. *JACC Basic Transl Sci* **4**, 449-467 (2019).

66. Fu X*, et al.* Specialized fibroblast differentiated states underlie scar formation in the infarcted mouse heart. *J Clin Invest* **128**, 2127-2143 (2018).

67. Whitesell TR*, et al.* An alpha-smooth muscle actin (acta2/alphasma) zebrafish transgenic line marking vascular mural cells and visceral smooth muscle cells. *PloS one* **9**, e90590 (2014).

68. Gupta V, Poss KD. Clonally dominant cardiomyocytes direct heart morphogenesis. *Nature* **484**, 479-484 (2012).

69. Lavoie H, Gagnon J, Therrien M. ERK signalling: a master regulator of cell behaviour, life and fate. *Nature reviews Molecular cell biology* **21**, 607-632 (2020).

70. Foglia B, Cannito S, Bocca C, Parola M, Novo E. ERK Pathway in Activated, Myofibroblast-Like, Hepatic Stellate Cells: A Critical Signaling Crossroad Sustaining Liver Fibrosis. *Int J Mol Sci* **20**, (2019).

71. Favata MF*, et al.* Identification of a novel inhibitor of mitogen-activated protein kinase kinase. *The Journal of biological chemistry* **273**, 18623-18632 (1998).

72. Cohen O, Granek R. Nucleus-targeted drug delivery: theoretical optimization of nanoparticles decoration for enhanced intracellular active transport. *Nano Lett* **14**, 2515-2521 (2014).

73. Fu A, Tang R, Hardie J, Farkas ME, Rotello VM. Promises and pitfalls of intracellular delivery of proteins. *Bioconjug Chem* **25**, 1602-1608 (2014).

74. Shaw S, Sarkar AK, Jana NR. Protein Delivery to the Cytosol and Cell Nucleus via Micellar Nanocarrier-Based Nonendocytic Uptake. *ACS Appl Bio Mater*, (2023).

75. Travers JG, Kamal FA, Robbins J, Yutzey KE, Blaxall BC. Cardiac Fibrosis: The Fibroblast Awakens. *Circulation research* **118**, 1021-1040 (2016).

76. Gonzalez-Rosa JM, Burns CE, Burns CG. Zebrafish heart regeneration: 15 years of discoveries. *Regeneration (Oxf)* **4**, 105-123 (2017).

77. Ross Stewart KM, Walker SL, Baker AH, Riley PR, Brittan M. Hooked on heart regeneration: the zebrafish guide to recovery. *Cardiovascular research* **118**, 1667-1679 (2022).

78. Csobonyeiova M, Beerova N, Klein M, Debreova-Cehakova M, Danisovic L. Cell-Based and Selected Cell-Free Therapies for Myocardial Infarction: How Do They Compare to the Current Treatment Options? *Int J Mol Sci* **23**, (2022).

79. Hashimoto H, Olson EN, Bassel-Duby R. Therapeutic approaches for cardiac regeneration and repair. *Nat Rev Cardiol* **15**, 585-600 (2018).

80. Trepicchio WL, Bozza M, Bouchard P, Dorner AJ. Protective effect of rhIL-11 in a murine model of acetaminophen-induced hepatotoxicity. *Toxicol Pathol* **29**, 242-249 (2001).

81. Zhao L*, et al.* Notch signaling regulates cardiomyocyte proliferation during zebrafish heart regeneration. *Proceedings of the National Academy of Sciences of the United States of America* **111**, 1403-1408 (2014).

82. Ng B*, et al.* Interleukin-11 is a therapeutic target in idiopathic pulmonary fibrosis. *Science translational medicine* **11**, (2019).

83. Yang W*, et al.* Interleukin-11 regulates the fate of adipose-derived mesenchymal stem cells via STAT3 signalling pathways. *Cell Prolif* **53**, e12771 (2020).

84. Kimura R*, et al.* Identification of cardiac myocytes as the target of interleukin 11, a cardioprotective cytokine. *Cytokine* **38**, 107-115 (2007).

85. Sweeney M*, et al.* Cardiomyocyte-Restricted Expression of IL11 Causes Cardiac Fibrosis, Inflammation, and Dysfunction. *Int J Mol Sci* **24**, (2023).

86. Chen CH, Durand E, Wang J, Zon LI, Poss KD. zebraflash transgenic lines for in vivo bioluminescence imaging of stem cells and regeneration in adult zebrafish. *Development* **140**, 4988-4997 (2013).

87. Lawson ND, Weinstein BM. In vivo imaging of embryonic vascular development using transgenic zebrafish. *Developmental biology* **248**, 307-318 (2002).

88. Proulx K, Lu A, Sumanas S. Cranial vasculature in zebrafish forms by angioblast cluster-derived angiogenesis. *Developmental biology* **348**, 34-46 (2010).

89. Wang J, Cao J, Dickson AL, Poss KD. Epicardial regeneration is guided by cardiac outflow tract and Hedgehog signalling. *Nature* **522**, 226-230 (2015).

90. Gemberling M, Karra R, Dickson AL, Poss KD. Nrg1 is an injury-induced cardiomyocyte mitogen for the endogenous heart regeneration program in zebrafish. *eLife* **4**, (2015).

91. Chablais F, Jazwinska A. Induction of myocardial infarction in adult zebrafish using cryoinjury. *J Vis Exp*, (2012).

92. Keating M, Hagle R, Osorio-Mendez D, Rodriguez A, Almutawa S, Kang J. A robust knock-in approach using a minimal promoter and a minicircle. *bioRxiv*, 2023.2009.2015.558008 (2023).

93. Sehring I, Mohammadi HF, Haffner-Luntzer M, Ignatius A, Huber-Lang M, Weidinger G. Zebrafish fin regeneration involves generic and regeneration-specific osteoblast injury responses. *eLife* **11**, (2022).

94. Begeman IJ*, et al.* Decoding an organ regeneration switch by dissecting cardiac regeneration enhancers. *Development* **147**, (2020).

95. Patra C, Kontarakis Z, Kaur H, Rayrikar A, Mukherjee D, Stainier DYR. The zebrafish ventricle: A hub of cardiac endothelial cells for in vitro cell behavior studies. *Sci Rep* **7**, 2687 (2017).

96. Kim D, Paggi JM, Park C, Bennett C, Salzberg SL. Graph-based genome alignment and genotyping with HISAT2 and HISAT-genotype. *Nature biotechnology* **37**, 907-915 (2019).

97. Liao Y, Smyth GK, Shi W. featureCounts: an efficient general purpose program for assigning sequence reads to genomic features. *Bioinformatics* **30**, 923-930 (2014).

98. Love MI, Huber W, Anders S. Moderated estimation of fold change and dispersion for RNA-seq data with DESeq2. *Genome biology* **15**, 550 (2014).

99. Wu T*, et al.* clusterProfiler 4.0: A universal enrichment tool for interpreting omics data. *Innovation (N Y)* **2**, 100141 (2021).

100. Rao A*, et al.* The translation initiation factor homolog eif4e1c regulates cardiomyocyte metabolism and proliferation during heart regeneration. *Development* **150**, (2023).

101. Stuart T*, et al.* Comprehensive Integration of Single-Cell Data. *Cell* **177**, 1888-1902 e1821 (2019).

FIGURES AND FIGURE LEGENDS

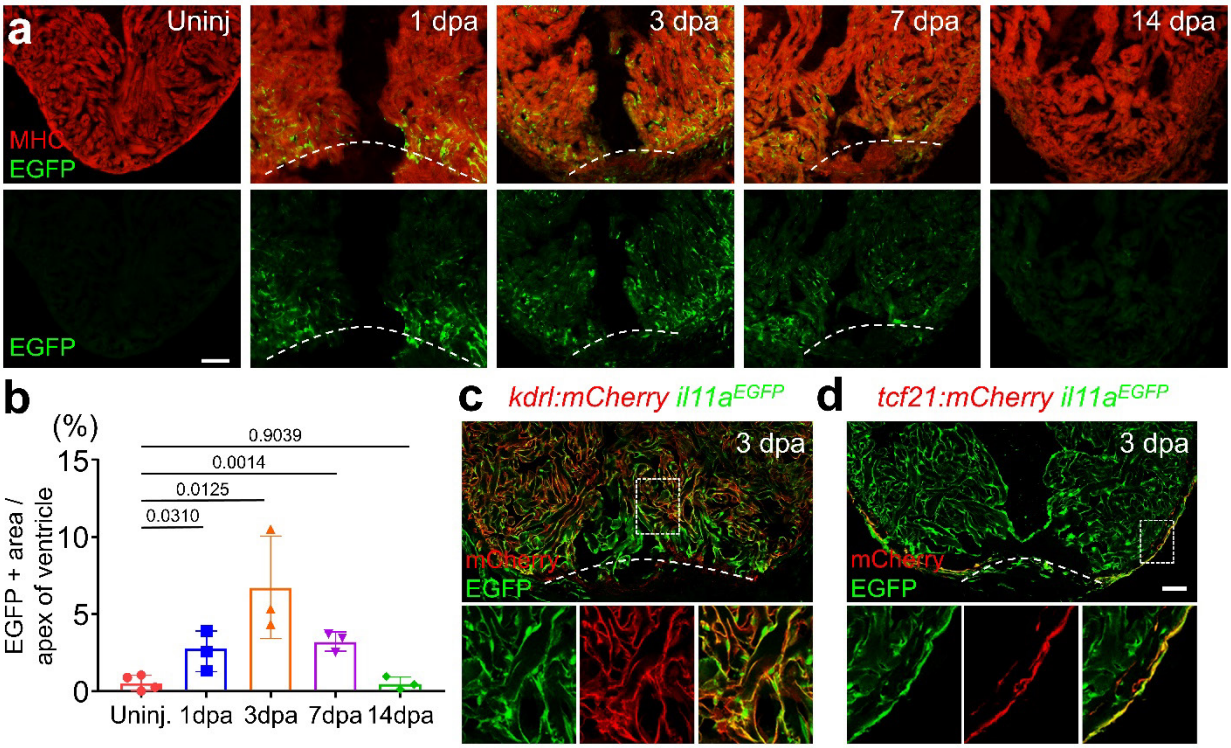

Figure 1. Spatiotemporal *il11a* expression during heart regeneration in adult zebrafish. (**a**) Representative cardiac section images of *il11a*^{EGFP}. Uninj, Uninjured. dpa, days post-amputation. (**b**) Quantification of EGFP expression area near the wound area. n = 3 - 4. (**c, d**) Comparison of *il11a*^{EGFP} expressing cells with *kdrl:mCherry* (**c**) and *tcf21:mCherry* (**d**) in 3 dpa hearts. *kdrl:mCherry* and *tcf21:mCherry* represent endocardium and epicardium, respectively. Dash boxes correspond to the region magnified in the panels below. Dotted lines demarcate the amputation plane. Scale bars, 100 μm in **a**, 50 μm in **d**.

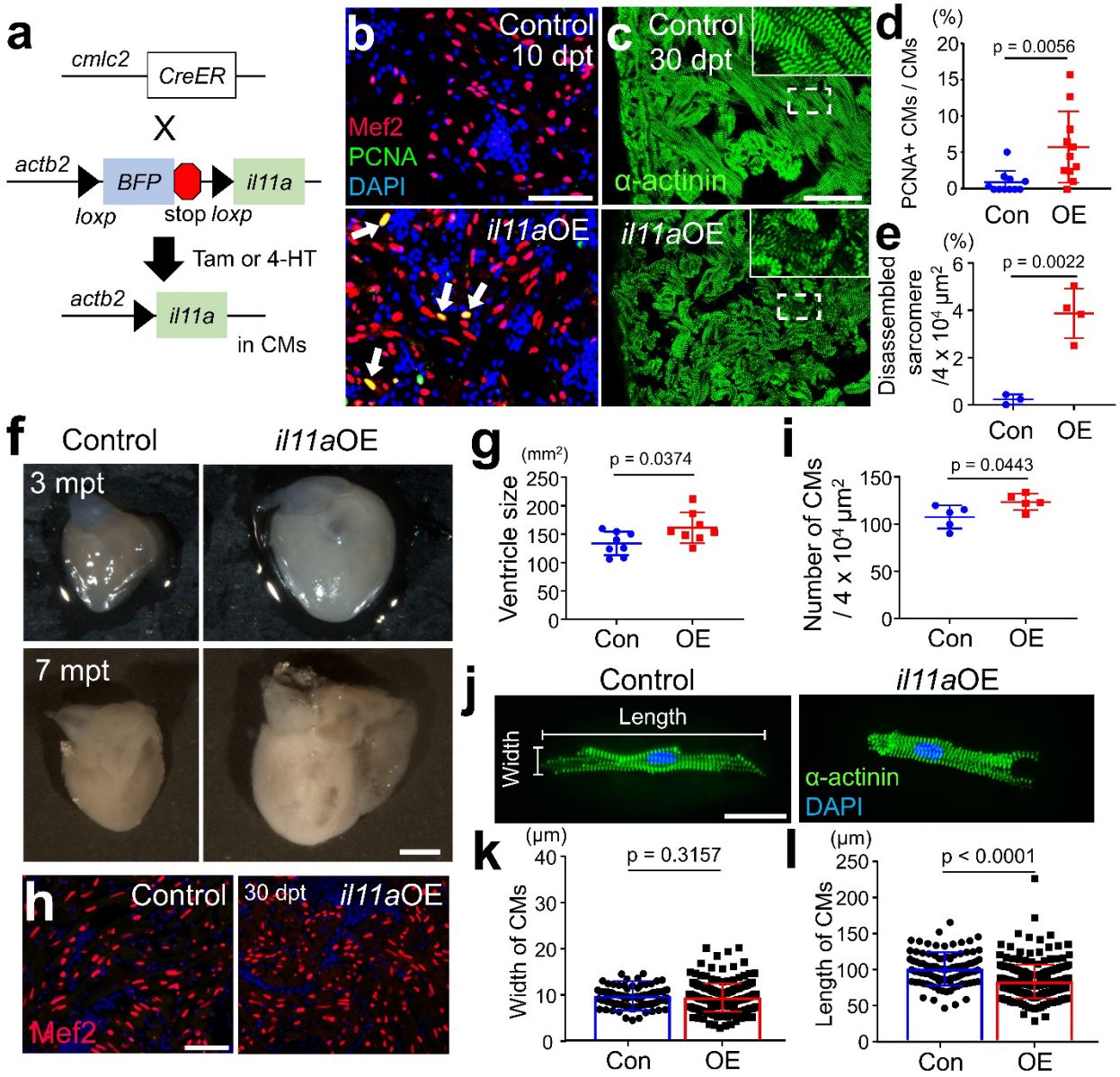

Figure 2. Myocardial *il11a* overexpression (OE) triggers CM proliferation in the absence of injury. (**a**) Schematic of tamoxifen (Tam) or 4-HT (4-Hydroxytamoxifen) inducible *il11a* overexpression (OE). *Tg*(*actb2:loxp-TagBFP-STOP-Loxp-il11a)*; *cmlc2:CreER* were administered with Tam or 4-HT to overexpress *il11a* (*il11a*OE). *Cre*-negative littermates were used as controls. (**b**) Representative cardiac section images stained with Mef2 (Red) and PCNA (Green) from control and *il11a*OE at 10 days post-treatment (dpt). Arrows indicate proliferative CMs. (**c**) Representative cardiac sections

images stained with α-actinin (green) from control and *il11a*OE uninjured hearts at 30 dpt. Insets correspond to higher magnifications of dashed boxes. (**d**) The percentage of PCNA$^+$ CMs of uninjured hearts from control (Con) and *il11a*OE (OE) at 7 dpt. n = 11. (**e**) Quantification of disorganized sarcomere structures in the ventricles of Con and *il11a*OE at 30 dpt. n = 3 - 4. (**f**) Whole-mount images of 3 and 7 months post-treatment (mpt) hearts from Con and *il11a*OE. (**g**) Quantification of the ventricle size from 3 mpt Con and *il11a*OE. n = 8. (**h**) Representative cardiac section images of 30 dpt control and *il11a*OE stained with Mef2 (red) and DAPI (blue). (**i**) Quantification for CM numbers in the ventricles from 30 dpt Con and *il11a*OE. n = 5. (**j**) Representative images of dissociated ventricular CMs stained with α-actinin (green) from 2 mpt control and *il11a*OE. (**k**, **l**) Quantification of the width (**k**) and the length (**l**) of individual CMs. n = 92 for Con and 234 for *il11a*OE. Scale bars, 50 μm in **b, c** and **h**, 0.5 mm in **f**, 25 μm in **j**.

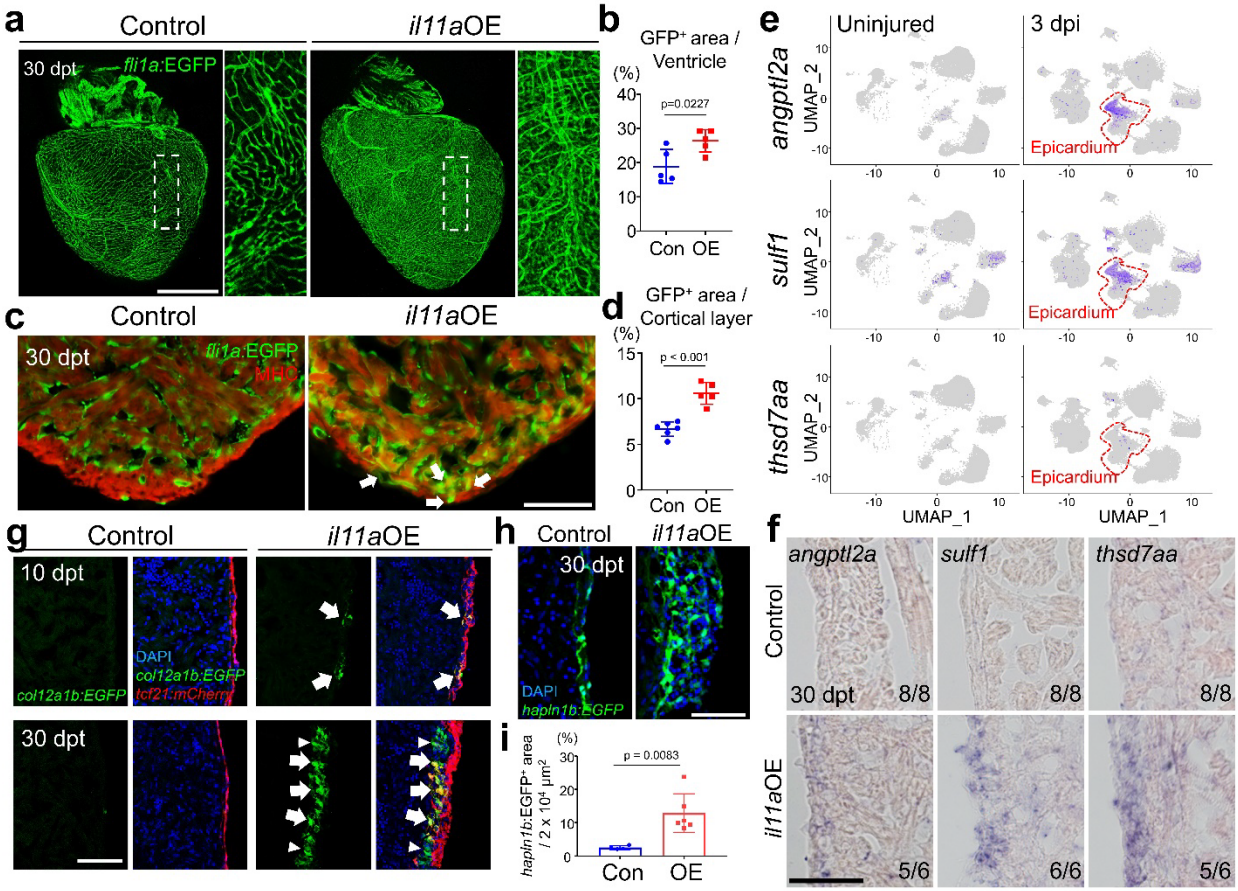

Figure 3. *il11a* induction stimulates vascularization in the absence of injury. (**a**) Representative whole-mount images of 30 dpt *fli1a:EGFP* hearts from control and *il11a*OE. Insets correspond to higher magnifications of dashed boxes. (**b**) Quantification of *fli1a:EGFP*⁺ vessel area in the ventricles for control Con and *il11a*OE. n = 5. (**c**) Representative cardiac section images of 30 dpt control and *il11a*OE hearts. Green and red indicate *fli1a*:EGFP and myosin heavy chain (MHC), respectively. Arrows indicate expanded EGFP⁺ region in the cortical layer. (**d**) Quantification of EGFP⁺ area in the cortical muscle layer from Con and *il11a*OE. n = 5 - 6. (**e**) Gene expression plots of *angptl2a, sulf1*, and *thsd7aa* induced in epicardium at 3 days post-injury (dpi). Cells expressing the indicated gene are colored purple, and the relative intensity indicates relative expression levels. Red dashed lines indicate epicardial expression of indicated

genes. uniform manifold approximation and projection (UMAP) clustering with annotated cell-types are in **Supplementary Fig. 6**. (**f**) Representative images of *in situ* hybridization (ISH) for angiogenic factors (*angptl2a*, *sulf1*, *thsd7aa*) on cardiac sections of control and *il11a*OE. The number in the lower right corner of each image represents the fraction of the analyzed hearts with displayed phenotype. n = 6 - 8. (**g**) Representative cardiac section images of control and *il11a*OE expressing *tcf21:mCherry; col12a1b:EGFP.* Top, 10 dpt. Bottom, 30 dpt. Blue, DAPI. Green, EGFP. Red, mCherry. n = 3 - 4. Arrows indicate *tcf21:mCherry* and *col12a1b:EGFP* double positive cells. Arrowheads indicate *tcf21:mCherry*$^{-}$*; col12a1b:EGFP*$^{+}$ cells. (**h**) Representative cardiac section images of 30 dpt control and *il11a*OE hearts. Green indicates *hapln1b*:EGFP. (**i**) Quantification of *hapln1b*:EGFP^{+} area in the cortical muscle layer from Con and *il11a*OE. n = 4 - 6. Scale bars, 500 μm in **a**, 50 μm in **c**, **f**, **g**, and **h**.

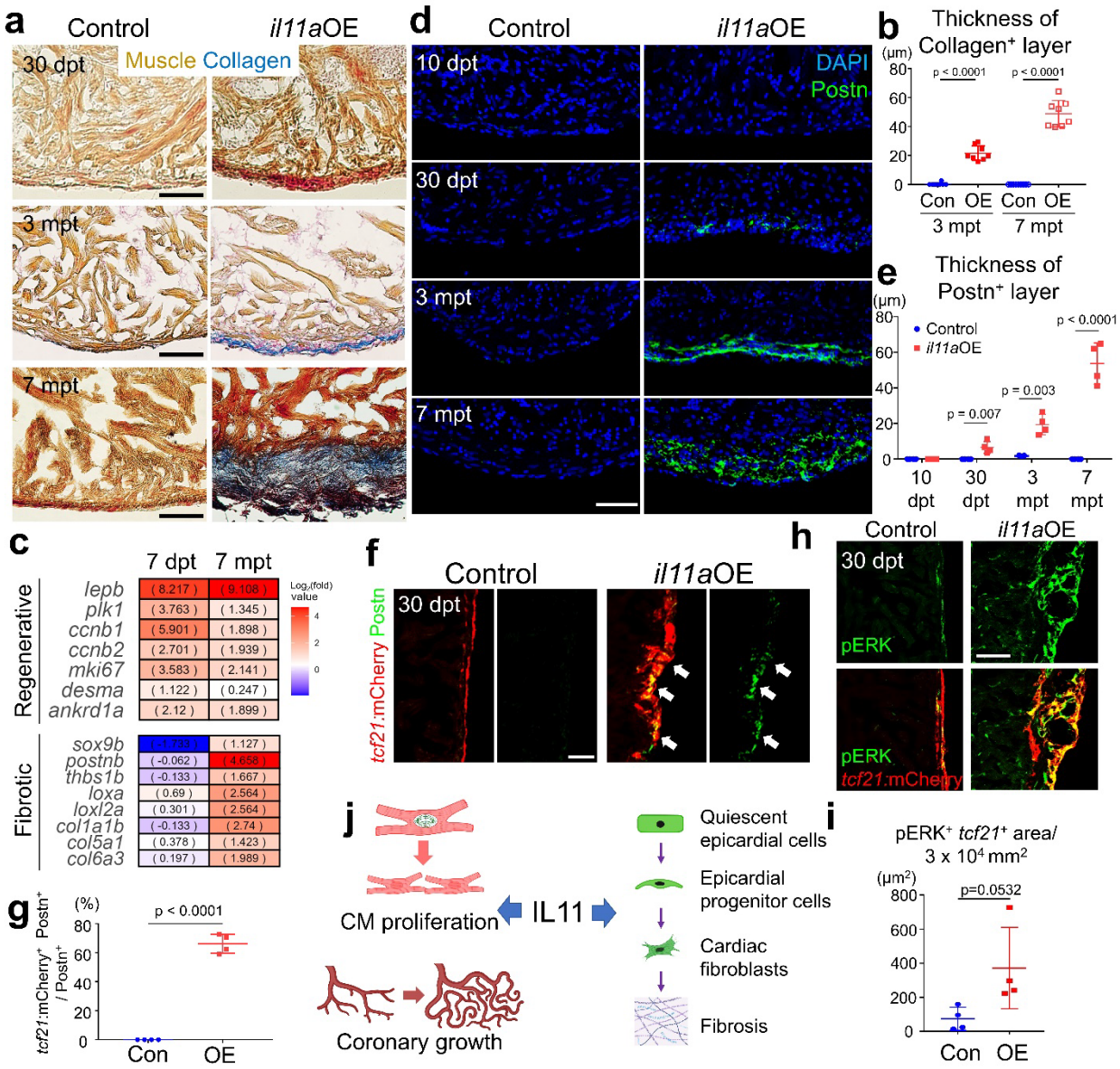

Figure 4. Fibrotic roles of *il11a* in adult zebrafish hearts. **(a)** Representative AFOG staining images of uninjured control and *il11a*OE hearts at 30 dpt (top), 3 mpt (middle), and 7 mpt (bottom). **(b)** Thickness of the collagen⁺ layer from Con and *il11a*OE at 3 and 7 mpt. n = 8 - 9**. (c)** Differential expression of genes associated with regeneration (top), cardiac fibroblasts and pathological fibrosis (bottom) between 7 dpt and 7 mpt. Gene associated with fibrosis and fibroblasts are significantly upregulated in 7 mpt *il11a*OE hearts, compared to control, while those genes are not induced in 7 dpt il11aOE hearts.

Expanded list of genes is in **Supplementary Fig. 7a**. **(d)** Representative cardiac section images of control and *il11a*OE hearts. Green and blue indicate Periostin (Postn)$^+$ fibroblasts and DAPI, respectively. **(e)** Thickness of the Postn$^+$ layer from Con and *il11a*OE at 10 and 30 dpt and 3 and 7 mpt. n = 3 - 4. **(f)** Representative images of cardiac sections labeled with Postn (green) and *tcf21*:mCherry (red) at 30 dpt. Arrows indicate *tcf21*$^+$ epicardial cells expressing Postn. **(g)** Colocalization assay of Postn$^+$ cells with *tcf21*:mCherry$^+$ layer. n = 4. (**h**) Representative cardiac section images stained with mCherry (red) and pERK (green) of 30 dpt Con and *il11a*OE hearts expressing *tcf21:mCherry*. (**i**) Quantification of pERK$^+$ area in *tcf21*$^+$ epicardium in the ventricles for Con and *il11a*OE. n = 4. (**j**) Dual roles of IL11 in the hearts. IL11 triggers cardiac regeneration programs, including CM proliferation and revascularization. Simultaneously, IL11 contributes to fibrosis by stimulating quiescent epicardial cells to generate epicardial progenitor cells (EPCs), which give rise to cardiac fibroblasts. Scale bars, 25 μm (top and middle) and 50 μm (bottom) in **a**, 50 μm in **d**, **f**, and **h**.

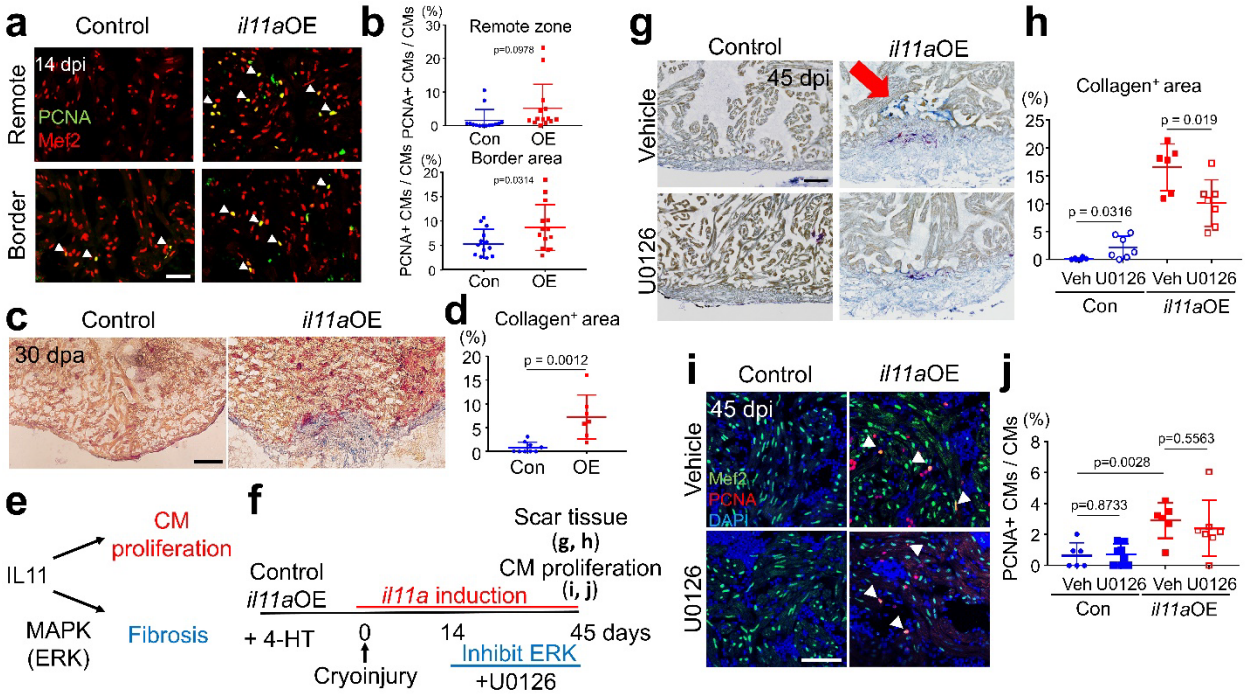

Figure 5. Combinatorial treatment enables to harness the regenerative potential of *il11a* in injured hearts. (a) Representative cardiac section images of 14 dpi control and *il11a*OE hearts stained with Mef2 (red) and PCNA (green). Cryoinjury was performed one day after administering four daily injections of 4-HT. Arrowheads indicate proliferative CMs. **(b)** The percentage of PCNA$^+$ CMs in the remote and border zone from Con and *il11a*OE at 14 dpi. n = 14. (**c**) Representative AFOG staining images of control and *il11a*OE hearts at 30 dpa. (**d**) Quantification of collagen$^+$ area in the ventricle of control Con and *il11a*OE at 30 dpa. n = 7 - 8. (**e**) Dual roles of *il11a* in injured hearts. *il11a* promotes CM proliferation while inducing fibrosis via Extracellular signal-regulated kinase (ERK) activity. (**f**) Experimental scheme to harness the regenerative potential of *il11a* while mitigating fibrosis by treating U0126, an ERK inhibitor, starting at 14 dpi. **(g)** Representative AFOG staining images of vehicle (Veh, 0.1% DMSO) or U0126 (10 μM) treated hearts from control and *il11a*OE. Hearts were collected at 45 dpi / 55 dpt. The arrow indicates the presence of scar tissue near the injury site in Veh-treated *il11a*OE

hearts. **(h)** Quantification of scar area in the ventricles of Veh or U0126-treated control and *il11a*OE hearts. n = 6 - 7. **(i)** Representative cardiac section images of Veh- or U0126-treated control and *il11a*OE hearts stained with Mef2 (green) and PCNA (red) at 45 dpi. Arrowheads indicate proliferative CMs. **(j)** The percentage of $PCNA^+$ CMs in the ventricles of Veh or U0126-treated control and *il11a*OE hearts at 45 dpi. n = 6 - 7. Scale bars, 25 μm in **a** and **g**, 50 μm in **c** and **i**.